Journal of Visualized Experiments

In vivo imaging of biological tissues with combined two-photon fluorescence and stimulated Raman scattering microscopy

--Manuscript Draft--

Article Type:	Methods Article - JoVE Produced Video
Manuscript Number:	JoVE63411R2
Full Title:	In vivo imaging of biological tissues with combined two-photon fluorescence and stimulated Raman scattering microscopy
Corresponding Author:	Sicong HE, Ph.D. Southern University of Science and Technology Shenzhen, Guangdong CHINA
Corresponding Author's Institution:	Southern University of Science and Technology
Corresponding Author E-Mail:	hesc@sustech.edu.cn
Order of Authors:	WANJIE WU
	XUESONG LI
	JIANAN QU
	SICONG HE
Additional Information:	
Question	**Response**
Please specify the section of the submitted manuscript.	Bioengineering
Please indicate whether this article will be Standard Access or Open Access.	Standard Access ($1400)
Please indicate the **city, state/province, and country** where this article will be **filmed**. Please do not use abbreviations.	Hong Kong, Kowloon
Please confirm that you have read and agree to the terms and conditions of the author license agreement that applies below:	I agree to the Author License Agreement
Please confirm that you have read and agree to the terms and conditions of the video release that applies below:	I agree to the Video Release
Please provide any comments to the journal here.	

TITLE:

In vivo Imaging of Biological Tissues with Combined Two-Photon Fluorescence and Stimulated Raman Scattering Microscopy

AUTHORS AND AFFILIATIONS:

Wanjie Wu[1], Xuesong Li[1], Jianan Y. Qu[1,2,3,4], Sicong He[5]

[1]Department of Electronic and Computer Engineering, The Hong Kong University of Science and Technology, Clear Water Bay, Kowloon, Hong Kong, P. R. China
[2]State Key Laboratory of Molecular Neuroscience, The Hong Kong University of Science and Technology, Clear Water Bay, Kowloon, Hong Kong, P. R. China
[3]Center of Systems Biology and Human Health, The Hong Kong University of Science and Technology, Clear Water Bay, Kowloon, Hong Kong, P. R. China
[4]Molecular Neuroscience Center, The Hong Kong University of Science and Technology, Clear Water Bay, Kowloon, Hong Kong, P.R. China
[5]Department of Biology, School of Life Sciences, Southern University of Science and Technology, Shenzhen, P.R. China

Email addresses of co-authors:
Wanjie Wu (wwuas@connect.ust.hk)
Xuesong Li (xliay@connect.ust.hk)
Jianan Y. Qu (eequ@ust.hk)
Sicong He (hesc@sustech.edu.cn)

Corresponding author:
Sicong He (hesc@sustech.edu.cn)

SUMMARY:

Stimulated Raman scattering (SRS) microscopy allows label-free imaging of biomolecules based on their intrinsic vibration of specific chemical bonds. In this protocol, the instrumental setup of an integrated SRS and two-photon fluorescence microscope is described to visualize cellular structures in the spinal cord of live mice.

ABSTRACT:

Stimulated Raman scattering (SRS) microscopy enables label-free imaging of the biological tissues in its natural microenvironment based on intrinsic molecular vibration, thus providing a perfect tool for *in vivo* study of biological processes at subcellular resolution. By integrating two-photon excited fluorescence (TPEF) imaging into the SRS microscope, the dual-modal *in vivo* imaging of tissues can acquire critical biochemical and biophysical information from multiple perspectives which helps understand the dynamic processes involved in cellular metabolism, immune response and tissue remodeling, etc. In this video protocol, the setup of a TPEF-SRS microscope system as well as the *in vivo* imaging method of the animal spinal cord is introduced. The spinal cord, as part of the central nervous system, plays a critical role in the

communication between the brain and peripheral nervous system. Myelin sheath, abundant in phospholipids, surrounds and insulates the axon to permit saltatory conduction of action potentials. *In vivo* imaging of myelin sheaths in the spinal cord is important to study the progression of neurodegenerative diseases and spinal cord injury. The protocol also describes animal preparation and *in vivo* TPEF-SRS imaging methods to acquire high-resolution biological images.

INTRODUCTION:

Raman microscopy[1,2] is emerging as a powerful label-free method to image biological tissues based on the characteristic frequencies of various chemical bonds in biomolecules. Owing to its non-invasive and well-adaptive imaging capability, Raman microscopy has been widely used for imaging lipid-enriched components in biological tissues like myelin sheath[3–5], adipocytes[6,7], and lipid droplets[8–10]. Stimulated Raman scattering (SRS) signal acquired as stimulated Raman gain (SRG) or stimulated Raman loss (SRL) is background-free, showing perfect spectral resemblance to spontaneous Raman scattering[11,12]. In addition, SRL and SRG are linearly dependent on the analyte concentration, allowing for quantitative analysis of biochemical components[9,11,13]. Two-photon excited fluorescence microscopy (TPEF) has been widely used for *in vivo* biological imaging owing to its inherent optical sectioning capability, deep penetration depth, and low phototoxicity[14–16]. However, the performance of TPEF imaging depends on the characteristics of fluorescent tags, and the number of resolvable colors is limited due to the broadband fluorescence spectra[8,17–19]. Label-free SRS imaging and fluorescence-based TPEF imaging are two complementary imaging modalities, and their combination can provide abundant biophysical and biochemical information of tissues. These two imaging modalities are both based on the nonlinear optical (NLO) processes, which allows simple integration in one microscope system. The combination of the SRS and TPEF imaging, the so-called dual-modal imaging, enables high-dimensional imaging and profiling of cells and tissues, facilitating a comprehensive understanding of complex biological systems. Specifically, picosecond (ps) SRS microscopy can achieve chemical-bond imaging with high spectral resolution compared with femtosecond (fs) SRS technique[11], allowing to differentiate multiple biochemical components in biological tissue, especially in the crowded fingerprint region[20,21]. In addition, compared with another commonly used dual-modal NLO microscope system with integration of coherent anti-Stokes scattering (CARS) microscope, SRS shows superior performance to CARS in terms of spectral and image interpretation as well as detection sensitivity[11]. The SRS-TPEF microscope has been used as a powerful tool to study various biological systems, such as *Caenorhabditis elegans*[9,22], *Xenopus laevis* tadpole brain[5], mouse brain[23,24], spinal cord[25,26], peripheral nerve[27], and adipose tissue[7], etc.

The spinal cord together with the brain makes up the central nervous system (CNS). Visualizing cellular activities in the CNS *in vivo* under physiological and pathological conditions is critical for understanding the mechanisms of CNS disorders[28–30] and for developing corresponding therapies[31–33]. Myelin sheath, which wraps and insulates axons for high-speed action potential conduction, plays a significant role in the development of the CNS. Demyelination is thought of as a hallmark in white matter disorders, such as multiple sclerosis[34] and spinal cord injury (SCI)[35]. In addition, after SCI, myelin debris can modulate macrophage activation, contributing to

chronic inflammation and secondary injury[36]. Therefore, *in vivo* imaging of myelin sheath together with neurons and glial cells in living mouse models is of great help to understand the dynamic processes in CNS disorders.

In this protocol, the fundamental setup procedures of a home-built TPEF-SRS microscope are described and the dual-modal *in vivo* imaging methods for mouse spinal cord are introduced.

PROTOCOL:

All animal procedures performed in this work are conducted according to the guidelines of the Laboratory Animal Facility of the Hong Kong University of Science and Technology (HKUST) and have been approved by the Animal Ethics Committee of HKUST. Safety training for laser handling is required to set up and operate the TPEF-SRS microscope. Always wear laser safety goggles with appropriate wavelength range when dealing with laser.

1. Setup of the TPEF-SRS microscope (for setup schematic see Figure 1)

1.1. Use an integrated optical parametric oscillator (OPO) connected with a mode-locked Ytterbium fiber laser as the picosecond (ps) laser source for SRS imaging.

NOTE: OPO outputs a Stokes beam (1031 nm) and a pump beam (tunable from 780 nm to 960 nm) with 2 ps pulse duration and 80 MHz repetition rate. The Stokes beam is modulated at 20 MHz by a built-in electro-optical modulator (EOM) for SRS high-frequency at MHz level phase-sensitive detection.

1.2. Use an fs titanium (Ti): sapphire laser as the laser source for TPEF imaging.

1.3. Use a pair of lenses (L1 and L2) to collimate and adjust the size of the fs beam to 3 mm.

1.4. Use a pair of achromatic doublets (L3 and L4) to collimate the ps laser beam and expand its diameter to 3 mm.

1.5. Change the polarization of the fs laser beam from p polarization to s polarization using a half-wave plate.

1.6. Combine the two laser beams with a polarizing beam splitter (PBS).

1.7. Add a pair of 3 mm XY-scan galvanometer mirrors behind the PBS for beam scanning.

1.8. Use a telecentric scan lens (L5) and an infinity-corrected tube lens (L6) to conjugate the scanning mirror and the rear pupil of the 25x objective lens. Expand the laser beam by the scan lens and tube lens to fill the back aperture of the objective.

1.9. Place a PBS or dichroic mirror (D2) between the tube lens and objective lens for SRS or

fluorescence signal collection. Use a motorized flipper to switch between PBS and D2.

NOTE: Part of the back-scattered SRS signal is lost when passing through the PBS as a result of its randomly shifted polarization.

1.10. Use a pair of lenses (L7 and L9) to narrow the detection beam and conjugate the rear pupil of the 25x objective lens with a photodiode sensor.

1.11. Use a pair of lenses (L8 and L10) to narrow the detection beam and conjugate the rear pupil of the 25x objective with the detection surface of the photomultiplier (PMT).

1.12. Use a dichroic mirror (D3) to separate the detection path of fluorescence and SRS signals.

1.13. Place a filter set (Fs1) in front of the photodiode detector to block the Stokes laser and pass the pump beam only.

1.14. Place a filter set (Fs2) in front of the PMT detector to pass the target fluorescence signal only.

1.15. Connect the PMT to a current amplifier for signal amplification.

1.16. Connect the photodiode to a lock-in amplifier.

1.18. Connect the sync signal from the built-in EOM output to the reference input of the lock-in frequency for SRS signal demodulation.

1.19. Connect the PMT amplifier and lock-in amplifier outputs to the data acquisition module.

2. TPEF-SRS microscope system calibration

2.1. Startup of the lasers

2.1.1. Switch the key switch from **Standby** to **On** position to turn on the Ti: sapphire laser and wait for 30 min for the laser to warm up.

2.1.2. Switch on the OPO by clicking on the **Start** button on the OPO control panel and wait for 20 min for the laser to warm up.

2.1.3. Lower the power of the Stokes beam to ~20 mW and place a high-speed photodetector at the OPO output to detect the beam. Connect the output port of the photodetector to the input port of an oscilloscope using a coaxial cable with Bayonet Neill-Concelman (BNC) connector to monitor the laser pulse.

2.1.4. After the ps laser warms up, use the high-speed photodetector to check the modulation depth of the Stokes beam.

2.1.5. Open the **EOM Control** window in the OPO control software. Adjust the EOM power and phase according to the pulse intensity diagram shown on the oscilloscope to achieve maximal modulation depth at 20 MHz.

NOTE: EOM performance is usually stable and only needs to be checked when the SRS signal is found significantly decreased.

2.2. Optical alignment of the combined TPEF-SRS microscope

2.2.1. Perform optical alignment for colocalization of the ps and fs beams as described in steps 2.2.2 to 2.2.13.

2.2.2. Open the pump laser shutter while stopping the Stokes output in the OPO control software. Use OPO control software to set the wavelength of the pump beam to 796 nm by clicking the **Set Signal** box and entering the wavelength value 796. Click on the **Set OPO Power Box** and enter 20 to set its power to the minimum (~20 mW) for optical alignment.

2.2.3. Switch on the microscope computer and all associated electronic components, including scanners, objective actuators, photodiodes, photomultiplier tubes (PMTs), current amplifiers, lock-in amplifiers, and motorized flippers. Start the microscope control software.

NOTE: The microscope control software is a homemade interface.

2.2.4. Place two alignment plates (P1 and P2 in **Figure 1**) in the optical path. Place P1 behind PBS at a distance of about 10 cm and place P2 behind P1 at a distance of about 30 cm.

NOTE: The ps and fs beams are combined using PBS (**Figure 1**). The two alignment plates are used to check the alignment as well as the colocalization of the two laser beams.

2.2.5. Open the microscope shutter for the ps laser beam.

2.2.6. Adjust the mirror M1 to locate the ps laser beam center at the through-hole of P1. Use an infrared (IR) scope to observe the position of the beam spot at P1 when adjusting the mirror M1.

2.2.7. Adjust the mirror M2 to locate the ps laser beam center at the through-hole of P2. Use the IR scope to observe the position of the beam spot at P2 when adjusting the mirror M2.

2.2.8. Repeat steps 2.2.6 and 2.2.7 until the ps beam center locates at the through-hole of both alignment plates. Close the shutter of the ps beam in the microscope control software.

2.2.9. Set the wavelength of fs Ti: sapphire laser at 740 nm and open the laser shutter. Set the laser power to 5 mW (measured at the input port of the microscope system) for optical alignment.

2.2.10. Open the microscope shutter for the fs laser beam.

2.2.11. Adjust the mirror M3 to locate the fs laser beam spot center at the through-hole of P1.

2.2.12. Adjust the mirror M4 to locate the laser beam spot center at the through-hole of P2.

2.2.13. Repeat steps 2.2.11 and 2.2.12 until the fs laser beam center locates at the through-holes of two alignment plates. Close the microscope shutter for the fs beam.

2.2.14. Perform spatial overlapping of the pump and Stokes beams as described in steps 2.2.15 to 2.2.18.

NOTE: Although the pump and Stokes beams are roughly overlapped inside the ps laser, fine-tuning of the positions of the two laser beams is required to achieve optimal SRS performance. Since the pump beam is firstly aligned as previously described, next the Stokes beam is adjusted to colocalize with the pump beam.

2.2.15. Place a camera at the position of the objective to visualize the location of two-beam spots. Mark the position of the pump beam on the camera screen as a reference.

2.2.16. Place an alignment plate P0 before L3 (**Figure 1**). Use a hex key to adjust the optical mirror 1 (OM1) so that the Stokes beam center passes the through-hole of the alignment plate at the laser output port. Use the IR scope to confirm the position of the beam spot at P0 during adjustment.

NOTE: OM1 and OM2 are two mirrors in the OPO head to adjust the position of the 1031 nm Stokes beam.

2.2.17. Remove the alignment plate P0 and use the hex key to adjust the OM2 so that the center of the Stokes beam colocalizes with the reference mark of the pump beam on the camera.

2.2.18. Repeat steps 2.2.16 and 2.2.17 until the Stokes beam strictly overlaps with the pump beam at both P0 and camera planes.

NOTE: When visualizing the beam spots on the camera, all the alignment plates should be removed from the optical path.

2.3. Optimize imaging conditions

2.3.1. Perform phase adjustment of the lock-in amplifier as described in steps 2.3.2. to 2.3.7.

NOTE: SRS detection is based on a high-frequency phase-sensitive scheme. For SRL detection, the intensity of the Stokes beam is modulated at 20 MHz and a lock-in amplifier is used to demodulate the signal. The phase and offset of the lock-in amplifier need to be adjusted to achieve the optimal image contrast.

2.3.2. Open the lock-in amplifier control software.

2.3.3. Set the wavelength of the pump laser to 796 nm and the power of the pump and Stokes beam to be 15 mW and 25 mW on the sample, respectively.

NOTE: Here use olive oil for SRS imaging optimization and calibration. The Raman peak of olive oil at the carbon-hydrogen region is at 2863.5 cm^{-1}, corresponding to the pump beam wavelength at 796 nm.

2.3.4. Place the olive oil sample on the stage and adjust the focus of the 25x objective onto the sample. Seal the olive oil in a slide. Attach a folded tissue paper to the bottom of the slide during signal detection to enhance the signal backscattering for epi-SRS detection.

2.3.5. Use the microscope control software to set the following imaging parameters for olive oil imaging as follows: 512 x 512 pixels for 500 µm x 500 µm field of view (FOV), 6.4 µs pixel dwell time. Use the lock-in amplifier control software to set the time constant value to be 10 µs, which is close to the pixel dwell time.

2.3.6. Scan the laser beam over the sample. Use the lock-in amplifier control software to tune the phase (0–180°) with a step size of 22.5° until the SRS signal intensity reaches the maximum.

NOTE: In this all-analog lock-in amplifier, the signal output is the in-phase component, which is dependent on the phase of the reference signal. The phase can be adjusted by the lock-in amplifier control software with 11° resolution, allowing to maximize the detected signal to within ~2%[12]. The lock-in amplifier gets out of phase once the sync signal is disrupted. The phase needs to be readjusted every time the sync signal is reestablished.

2.3.7. Scan the sample with laser shutter closed. Use the lock-in amplifier control software to tune the offset value with a step size of 1 mV until the average SRS signal is close to zero.

NOTE: The average SRS signal is estimated as the average intensity of all pixels in the SRS image, which is calculated automatically by the microscope control software. Offsets are useful for canceling unwanted phase-coherent signals.

2.3.8. Perform temporal synchronization optimization as described in steps 2.3.9 to 2.3.14.

2.3.9. Open the **Delay Manager** dialog (**Figure 2**) in the **OPO Control** software.

2.3.10. Scan the olive oil and tune the delay stage until the olive oil SRS signal reaches its maximum.

NOTE: For the first time of SRS imaging, when the phase of the lock-in amplifier has not been optimized, temporal synchronization is first roughly adjusted to visualize the SRS signal of the sample before optimizing the phase of the lock-in amplifier.

2.3.11. Stop scanning and click on the **Add Data** button in the delay manager dialogue to record the current delay data.

2.3.12. Repeat steps 2.3. 10 and 2.3.11 for different chemical samples at different wavelengths.

NOTE: Polystyrene beads, heavy water, 5-Ethynyl-2'-deoxyuridine, glycerol are used to measure the delay data at different vibrational bands.

2.3.13. Select the **Data Fit** and **Order 5** on the delay manager dialogue to fit the current data points with the fifth-order polynomic function. Apply the fitted data by clicking on the **Use As Custom** button and checking the check box. The delay stage will be auto-adjusted at different wavelengths according to the fitted delay curve.

2.3.14. Save all the delay data in a text file, which can be loaded for future use.

3. Surgical preparation of mouse for *in vivo* fluorescence and SRS imaging

3.1. Sterilize all required tools, including spring scissors, forceps, coverslips, and gauze pads.

3.2. Disinfect all the surfaces, which would be touched during surgery with 70% ethanol. Cover the working area of the benchtop with disinfected drapes. Put a heating pad under the drape.

3.3. Use Thy1-YFP-H (Tg(Thy1-YFP)HJrs/J)[37] transgenic mice that express enhanced yellow fluorescence protein (EYFP) in dorsal root ganglion afferent neurons for *in vivo* spinal cord imaging. Weigh the mouse and induce anesthetization by intraperitoneal (i.p.) injection of the ketamine-xylazine mixture (87.5 mg kg^{-1} and 12.5 mg kg^{-1}).

3.4. Pinch the toe of the mouse to ensure deep anesthesia. Supplement with half the original dose of the anesthetics if needed. Apply ointment to the mouse eyes to prevent corneal dryness.

3.5. Shave the hair on the back above the thoracic spine, and then completely remove the hair using a depilating cream. Disinfect the shaved area with iodine solution.

3.6. Make a small midline incision (~1.5 cm) of the skin over the T11–T13 vertebra with a

scalpel.

3.7. Severe muscles and tendons both on top and on sides of the T11–T13 vertebra with spring scissors and forceps. Expose the three adjacent vertebras. Use sterile gauze pads and sterile saline to control bleeding and to clean the surgical site.

3.8. Stabilize the spine with the help of the two stainless steel sidebars on a custom-designed stabilization stage (**Figure 2B**).

3.9. Use a #2 forceps to perform a laminectomy at T12. Carefully use the forceps to break the lamina piece by piece until the whole lamina of the T12 vertebra is removed.

3.10. Wash away the blood overlying the spinal cord with sterile saline and use the gauze pad to absorb excessive fluid. Apply pressure on the bleeding site with a piece of gauze pad to control bleeding.

3.11. Place a coverslip (22 x 22 mm) on the clamping bar and fill the interspace between the coverslip and the spinal cord with saline.

4. *In vivo* TPEF-SRS imaging of mouse spinal cord

4.1. Mount the stabilization stage on a five-axis stage beneath the TPEF-SRS microscope.

NOTE: The five-axis stage allows three-axis translation and ±5° pitch and roll flexure motion.

4.2. Secure the mouse head with two head bars and lower the holding plate to offer enough space for chest movement during breathing, alleviating motion artifacts.

4.3. Insert a heating pad under the mouse to keep the mouse warm during imaging.

4.4. Adjust the z translational stage to tune the focus until the bright-field image of spinal cord vasculature can be observed under a 10x objective.

4.5. Locate the spinal cord dorsal vein at the center of the FOV by tuning the two-axis translational stage of the five-axis stage.

4.6. Tune the roll and pitch angles of the five-axis stage to adjust the spinal cord dorsal surface perpendicular to the objective axis based on the bright-field image.

4.7. Replace the 10x with a 25x water immersion objective for TPEF-SRS imaging.

4.8. Set the wavelength of the fs beam to 920 nm. Tune the fs beam power to be 10 mW for the 25x objective.

4.9. Set the wavelength of the pump beam to 796 nm. Tune the power of the pump and Stokes beam to be 60 mW and 75 mW on the sample, respectively.

NOTE: Spinal cord SRS imaging is performed at the wavenumber of 2863.5 cm^{-1}, which corresponds to the Raman peak of myelin sheaths at the carbon-hydrogen region based on the measured SRS spectra[7,9]. The laser power is determined to ensure high-resolution and high-contrast spinal cord images in both fluorescence and SRS imaging modalities. Tissue damage is not observed under the current imaging conditions

4.10. For SRS imaging, select PBS above the objective using a motorized flipper by pressing the **Switch** button connected to the motorized flipper.

4.11. Set the imaging parameters as follows: 512 x 512 pixels for 150 µm x 150 µm FOV, 3.2 µs pixel dwell time, 2 µs time constant.

4.12. Start scanning the sample and set the focus on the dorsal surface of the spinal cord.

4.13. Finely tune the delay stage by the OPO control software until maximum spinal cord SRS signal is achieved.

NOTE: Biological samples can induce extra chromatic dispersion, the delay stage may require to be adjusted to optimize the temporal synchronization. However, when SRS imaging is performed near the tissue top surface, the temporal difference of the two laser pulses introduced by the biological tissue and the imaging window is usually small (less than several hundred fs).

4.14. For TPEF imaging, select dichroic mirror D2 above the objective using a motorized flipper by pressing the **Switch** button connected to the motorized flipper.

4.15. Set the imaging parameters and start scanning the sample. To capture the TPEF-SRS image stack, acquire the TPEF and SRS images sequentially with a 1 s interval at the same depth before going to the next depth. The imaging parameters for TPEF imaging are 512 x 512 pixels, 150 µm x 150 µm FOV, 3.2 µs pixel dwell time.

4.16. Remove animals from the stabilization stage after all images are collected.

4.17. Clean the exposed tissue by flushing saline and absorb the excess fluid using a gauze pad. Apply silicone gel on the exposed spinal cord and wait for ~5 min until it gets cured.

4.18. Suture the skin with #6-0 surgical suture to close the wound. Apply burn cream on the skin of the surgical site to prevent infection.

4.19. Place the animal in a clean cage and place the cage on a heating pad until the mouse fully recovers from anesthesia.

4.20. Close the shutter of OPO and fs laser. Set the power of the pump and Stokes beam to the maximum.

NOTE: Setting maximal power before turning off the laser is beneficial for laser maintenance.

4.21. Set the wavelength of the pump beam and fs laser to 800 nm.

4.22. Set the two lasers on standby, close all the electronics control software and turn off all the associated equipment.

REPRESENTATIVE RESULTS:

In vivo dual-modal imaging of spinal axons as well as myelin sheaths is conducted using the Thy1-YFPH transgenic mice, which express EYFP in dorsal root ganglion afferent neurons (**Figure 3**). These labeled afferent neurons relay the sensory information from the peripheral nerve to the spinal cord, with the central branch located in the spinal cord dorsal column. With the TPEF-SRS microscope, densely distributed myelin sheath can be clearly visualized in the dorsal column using label-free SRS imaging, and sparsely labeled YFP axons are observed using TPEF imaging. It is revealed by the dual-model imaging that axons are closely wrapped by a thick layer of myelin sheaths. Nodes of Ranvier (NR), where the axolemma is bare of the myelin sheath, play an essential role in the fast saltatory propagation of action potentials. As can be seen in the spinal cord image (**Figure 3C**), NR can be visualized by TPEF-SRS imaging with the axonal diameter significantly decreased and the axolemma directly exposed to the extracellular matrix. It is essential to image the axons together with the surrounding myelin sheaths to confirm the existence and location of NR. Therefore, TPEF-SRS microscopy allows us to observe the dynamic changes of axons and myelin sheaths in the development of spinal cord disorders, which is significant to understand the mechanisms of cellular dynamics.

FIGURE AND TABLE LEGENDS:

Figure 1: The schematic diagram of the TPEF-SRS microscope system. The pump and Stokes beams are combined with a dichroic mirror (D1) in the picosecond (ps) laser. The ps beam and femtosecond (fs) beam are collimated and expanded/narrowed by a pair of lenses (L1, L2, and L3, L4, respectively) to match the 3 mm XY-scan galvanometer mirrors. The fs beam is rotated from horizontal to vertical polarization by a half-wave plate (HWP), and then combined with the ps beam by a polarizing beam splitter (PBS). The scanning mirrors and the rear pupil of the objective lens are conjugated by a telecentric scan lens L5 and an infinity-corrected tube lens L6. The laser beam is expanded by the scan and tube lens to fill the back aperture of the 25x objective. For stimulated Raman scattering (SRS) imaging, the backscattered pump beam collected by the objective is reflected by a PBS and directed to a large area (10 mm x 10 mm) silicon photodiode (PD). For two-photon imaging, the two-photon excited fluorescence (TPEF) signal is reflected by a dichroic beam splitter D2 to the photodetection unit. A current photomultiplier (PMT) module is used to detect the TPEF signal. Abbreviations—L1–L10: lenses; OL: objective lens; D1–D3: dichroic mirrors; Fs1, Fs2: filter sets; M: mirrors; OM1, OM2: optical mirrors; P0–P2: alignment plates.

Figure 2: The interface of the delay manager on the OPO control software. The red arrow indicates the checking box for applying the calibrated delay data.

Figure 3: *In vivo* TPEF-SRS imaging of mouse spinal cord. (**A**) Schematic diagram of the surgical preparation of the mouse spinal cord and the bright-field image of the spinal cord. (**B**) Mouse mounting scheme for *in vivo* imaging of spinal cord. (**C**) Maximal z projection images of axons and myelin sheaths in mouse spinal cord. White arrowheads indicate the location of a node of Ranvier. SRS images of myelin are taken at the Raman shift of 2863.5 cm^{-1}.

DISCUSSION:

In this protocol, the basic setup of the TPEF-SRS microscope is described in detail. For SRS imaging, the pump and Stokes beams are temporally and spatially overlapped inside the OPO; this overlapping can be disrupted after passing through the microscope system. Therefore, both spatial and temporal optimization of the colocalization of the pump and Stokes beams is necessary and critical to achieving optimal SRS imaging. The temporal delay between the pump and Stokes beam is related to the optical path difference, which is determined by the dispersion of optical elements in the microscope system[38]. When the wavelength of the pump beam is tuned for SRS imaging at different Raman shifts, the optical path length of the pump beam changes accordingly because the refractive index of the optical lens is dependent on the wavelength[38]. Therefore. the temporal delay between the pump and Stokes laser pulse changes with the wavelength of the pump beam and thus needs to be calibrated. The OPO is equipped with a software-controlled delay line, which can be used to compensate for the time delay between the pump and Stokes beams. The internal delay inside the OPO has already been compensated based on the factory-calibrated data. The external dispersion introduced by the microscope system requires additional compensation. For the same optical path, the delay data remains stable and only needs to be calibrated once. As a result, the delay data at different wavelengths of the pump beam can be saved at the first measurement for future use. The calibrated delay data can be applied automatically by the OPO control software when the wavelength of the pump beam is changed, which is convenient for SRS imaging at different Raman shifts or hyperspectral SRS imaging. For TPEF-SRS imaging, strict spatial overlapping of the ps and fs beams after the combination is a critical step to avoid any FOV shift between the two imaging models. In this TPEF-SRS microscope, three beams are involved in the spatial colocalization. Firstly, the ps pump beam and fs beam are aligned to make sure they are both on the optical axis of the microscope system. Then, using the pump beam as a reference, the Stokes beam position is adjusted accordingly to achieve strict spatial colocalization. Each alignment procedure requires several trials to reach the optimum.

If the SRS signal significantly decreases, the phase value of the lock-in amplifier and time-delay data should be checked first. Since the lock-in amplifier gets out of phase once the sync signal is disrupted, the phase value requires readjusting every time after its power supply or EOM sync signal is interrupted. The temporal synchronization of the pump and Stokes beam can be quickly checked by slightly adjusting the delay line inside the OPO. If the calibrated time-delay data is far away from the optimal value, a zero scan should be performed to recalibrate the

delay offset by clicking the **Zero Scan** button on the delay manager dialogue. The whole zero scan procedure takes about 10 min. If the SRS signal fails to recover after the phase and time-delay value are optimized, the EOM modulation of the Stokes beam should be checked as described in steps 2.1.3–2.1.5. If the extinction ratio is far less than 10 dB with the observation of small pulse peaks at the off position of the Stokes pulse train, the EOM should be restarted and the modulation power and phase should be adjusted to achieve maximal modulation depth. Usually, the modulation problem can be solved by resetting the EOM. If not, technical support from the manufacturer should be required.

For *in vivo* thick tissue imaging, epi-SRS detection mode has to be used. In this protocol, a PBS is used to pass the excitation laser and reflect the back-scattered SRS signal to the detector. The detected SRL signal is dependent on the backscattering of the forward-going pump beam by tissues. Though the excitation lasers have linear polarization and can fully pass through the PBS, the backscattered beam has shifted polarization and can thus only be partially reflected by the PBS. Therefore, the current signal collection scheme shows lower efficiency compared to the strategy that directly places an annular photodetector in front of the objective[12]. Nevertheless, due to the strong scattering of the lipid-rich tissues[39], high signal-to-noise ratio SRS images (512 x 512 pixels) of the spinal cord can be acquired with 1–2 s integration time, making this PBS-based collection scheme an effective approach for spinal cord imaging. On the other hand, however, the strong tissue scattering also limits light penetration depth. For both SRS and TPEF imaging, the imaging depth for the spinal cord is limited to about 50 μm.

The sequential imaging procedure for SRS and TPEF imaging is the major limitation of the current dual-modal imaging method. In the protocol, TPEF and SRS imaging are performed at the same location sequentially with a 1 s interval by switching the motorized flipper automatically. Motion artifacts may cause an imperfect merge of the TPEF and SRS images, which limits the capability of this method for imaging highly dynamic processes or tissues largely affected by the breath and heartbeat of animals. One possible solution is to collect the ps laser-excited two-photon fluorescence simultaneously during SRS imaging[9]. However, this method is only applicable to the biological structures with strong fluorescence signals, since the ps pulse has a much lower fluorescence excitation efficiency compared to the fs pulse[14]. Alternatively, the motion problem can be solved using an fs-SRS system[22,40], where the fs laser source allows simultaneous excitation of the SRS and TPEF signals effectively, at the expense of low spectral resolution of the SRS imaging. Another solution is to use the ps laser-excited fluorescence obtained during SRS imaging as a reference to register the fs fluorescence images. As shown in **Figure 3**, this registration strategy works well if no significant motion occurs during the SRS and fluorescence imaging.

SRS exhibits unique advantages in biological imaging since it provides chemical information of biomolecules based on its specific label-free contrast mechanism[41]. Compared with CARS which has also been combined with TPEF for multimodal NLO imaging, SRS showed better spectral and image interpretation capability[11]; therefore, it has been widely applied for imaging lipid[9,11], protein[42,43], DNA[44], and bio-orthogonal components containing alkyne (C ≡ C)[13,45], carbon−deuterium (C−D)[9,46] and oxygen-deuterium (O-D) bonds[47,48] in biological tissues. In this

protocol, we used a ps laser source for SRS imaging and an fs laser source for TPEF imaging, which combines the advantages of high-efficiency fluorescence excitation and high Raman spectral resolution, allowing effective differentiation of diverse biomolecules[42,44]. In the spinal cord, complex cell-microenvironment interactions involving glial cells, neurons, and recruited immune cells contribute to the progression of injury[49] and diseases[50]. Combined with various fluorescence and SRS imaging probes, TPEF-SRS microscopy can achieve simultaneous imaging of various cellular structures as well as their distinct biomolecule components, which can significantly facilitate our understanding of the onset and development of spinal cord disorders.

ACKNOWLEDGMENTS:

This work was supported by the Hong Kong Research Grants Council through grants 16103215, 16148816, 16102518, 16102920, T13-607/12R, T13-706/11-1, T13-605/18W, C6002-17GF, C6001-19E, N_HKUST603/19, the Innovation and Technology Commission (ITCPD/17-9), the Area of Excellence Scheme of the University Grants Committee (AoE/M-604/16, AOE/M-09/12), and the Hong Kong University of Science & Technology (HKUST) through grant RPC10EG33.

DISCLOSURES:

The authors have nothing to disclose and have no competing financial interests.

REFERENCES:

1. Raman, C. V., Krishnan, K. S. The optical analogue of the compton effect. *Nature*. **121** (3053), 711 (1928).
2. Turrell, G., Corset, J. *Raman Microscopy: Developments and Applications*. Academic Press (1996).
3. Tian, F. et al. Monitoring peripheral nerve degeneration in ALS by label-free stimulated Raman scattering imaging. *Nature Communications*. **7** (1), 13283 (2016).
4. Shi, Y. et al. Longitudinal in vivo coherent anti-Stokes Raman scattering imaging of demyelination and remyelination in injured spinal cord. *Journal of Biomedical Optics*. **16** (10), 106012 (2011).
5. Hu, C.-R., Zhang, D., Slipchenko, M. N., Cheng, J.-X., Hu, B. Label-free real-time imaging of myelination in the Xenopus laevis tadpole by in vivo Stimulated Raman Scattering Microscopy. *Journal of Biomedical Optics*. **19** (8), 086005 (2014).
6. Den Broeder, M. J. et al. Altered adipogenesis in Zebrafish larvae following high fat diet and chemical exposure is visualised by Stimulated Raman Scattering Microscopy. *International Journal of Molecular Sciences*. **18** (4), 894 (2017).
7. He, S. et al. In vivo metabolic imaging and monitoring of brown and beige fat. *Journal of Biophotonics*. **11** (8), e201800019 (2018).
8. Wang, M. C., Min, W., Freudiger, C. W., Ruvkun, G., Xie, X. S. RNAi screening for fat regulatory genes with SRS microscopy. *Nature Methods*. **8** (2), 135–138 (2011).
9. Li, X. et al. Quantitative imaging of lipid synthesis and lipolysis dynamics in *Caenorhabditis elegans* by Stimulated Raman Scattering Microscopy. *Analytical Chemistry*. **91** (3), 2279–2287 (2019).
10. Zhang, C., Li, J., Lan, L., Cheng, J.-X. Quantification of lipid metabolism in living cells through the dynamics of lipid droplets measured by Stimulated Raman Scattering Imaging. *Analytical*

617 *Chemistry*. **89** (8), 4502–4507 (2017).
618 11. Freudiger, C. W. et al. Label-free biomedical imaging with high sensitivity by Stimulated
619 Raman Scattering Microscopy. *Science*. **322** (5909), 1857–1861 (2008).
620 12. Saar, B. G. et al. Video-rate molecular imaging in vivo with Stimulated Raman Scattering.
621 *Science*. **330** (6009), 1368–1370 (2010).
622 13. Li, X., Jiang, M., Lam, J. W. Y., Tang, B. Z., Qu, J. Y. Mitochondrial imaging with combined
623 fluorescence and Stimulated Raman Scattering Microscopy using a probe of the aggregation-
624 induced emission characteristic. *Journal of the American Chemical Society*. **139** (47), 17022–
625 17030 (2017).
626 14. Helmchen, F., Denk, W. Deep tissue two-photon microscopy. *Nature Methods*. **2** (12), 932–
627 940 (2005).
628 15. Pawlicki, M., Collins, H. A., Denning, R. G., Anderson, H. L. Two-photon absorption and the
629 design of two-photon dyes. *Angewandte Chemie International Edition*. **48** (18), 3244–3266
630 (2009).
631 16. König, K. Multiphoton microscopy in life sciences. *Journal of Microscopy*. **200** (2), 83–104
632 (2000).
633 17. Dean, K. M., Palmer, A. E. Advances in fluorescence labeling strategies for dynamic cellular
634 imaging. *Nature Chemical Biology*. **10** (7), 512–523 (2014).
635 18. Tsurui, H. et al. Seven-color fluorescence imaging of tissue samples based on fourier
636 spectroscopy and singular value decomposition. *Journal of Histochemistry & Cytochemistry*. **48**
637 (5), 653–662 (2000).
638 19. Niehörster, T. et al. Multi-target spectrally resolved fluorescence lifetime imaging
639 microscopy. *Nature Methods*. **13** (3), 257–262 (2016).
640 20. Zhang, X. et al. Label-free live cell imaging of nucleic acids using Stimulated Raman
641 Scattering (SRS) Microscopy. *Chemphyschem : A European Journal of Chemical Physics and*
642 *Physical Chemistry*. **13** (4), 1054–1059 (2012).
643 21. Ji, M. et al. Label-free imaging of amyloid plaques in Alzheimer's disease with stimulated
644 Raman scattering microscopy. *Science Advances*. **4** (11), eaat7715 (2018).
645 22. Li, X. et al. Integrated femtosecond stimulated Raman scattering and two-photon
646 fluorescence imaging of subcellular lipid and vesicular structures. *Journal of Biomedical Optics*.
647 **20** (11), 110501 (2015).
648 23. Imitola, J. et al. Multimodal coherent anti-Stokes Raman scattering microscopy reveals
649 microglia-associated myelin and axonal dysfunction in multiple sclerosis-like lesions in mice.
650 *Journal of Biomedical Optics*. **16** (2), 021109 (2011).
651 24. Uckermann, O. et al. Label-free multiphoton microscopy reveals altered tissue architecture
652 in hippocampal sclerosis. *Epilepsia*. **58** (1), e1–e5 (2017).
653 25. Tamosaityte, S. et al. Inflammation-related alterations of lipids after spinal cord injury
654 revealed by Raman spectroscopy. *Journal of Biomedical Optics*. **21** (6), 061008 (2016).
655 26. Uckermann, O. et al. Endogenous two-photon excited fluorescence provides label-free
656 visualization of the inflammatory response in the rodent spinal cord. *BioMed Research*
657 *International*. **2015**, 859084 (2015).
658 27. Hameren, G. van et al. In vivo real-time dynamics of ATP and ROS production in axonal
659 mitochondria show decoupling in mouse models of peripheral neuropathies. *Acta*
660 *Neuropathologica Communications*. **7** (1), 1–16 (2019).

661 28. Davalos, D. et al. Fibrinogen-induced perivascular microglial clustering is required for the
662 development of axonal damage in neuroinflammation. *Nature Communications*. **3** (1), 1–15
663 (2012).
664 29. Ylera, B. et al. Chronically CNS-injured adult sensory neurons gain regenerative competence
665 upon a lesion of their peripheral axon. *Current Biology*. **19** (11), 930–936 (2009).
666 30. Wake, H., Moorhouse, A. J., Jinno, S., Kohsaka, S., Nabekura, J. Resting microglia directly
667 monitor the functional state of synapses in vivo and determine the fate of ischemic terminals.
668 *Journal of Neuroscience*. **29** (13), 3974–3980 (2009).
669 31. Lau, S.-F. et al. IL-33-PU.1 transcriptome reprogramming drives functional state transition
670 and clearance activity of microglia in Alzheimer's Disease. *Cell Reports*. **31** (3), 107530 (2020).
671 32. Tang, P. et al. In vivo two-photon imaging of axonal dieback, blood flow, and calcium influx
672 with methylprednisolone therapy after spinal cord injury. *Scientific Reports*. **5**, 9691 (2015).
673 33. Yang, Z., Xie, W., Ju, F., khan, A., Zhang, S. In vivo two-photon imaging reveals a role of
674 progesterone in reducing axonal dieback after spinal cord injury in mice. *Neuropharmacology*.
675 **116**, 30–37 (2017).
676 34. Dobson, R., Giovannoni, G. Multiple sclerosis – a review. *European Journal of Neurology*. **26**
677 (1), 27–40 (2019).
678 35. Totoiu, M. O., Keirstead, H. S. Spinal cord injury is accompanied by chronic progressive
679 demyelination. *Journal of Comparative Neurology*. **486** (4), 373–383 (2005).
680 36. Kopper, T. J., Gensel, J. C. Myelin as an inflammatory mediator: Myelin interactions with
681 complement, macrophages, and microglia in spinal cord injury. *Journal of Neuroscience*
682 *Research*. **96** (6), 969–977 (2018).
683 37. Feng, G. et al. Imaging neuronal subsets in transgenic mice expressing multiple spectral
684 variants of GFP. *Neuron*. **28** (1), 41–51 (2000).
685 38. Pedrotti, F. L., Pedrotti, L. M., Pedrotti, L. S. Introduction to Optics. *Higher Education from*
686 *Cambridge University Press* (2017).
687 39. Jacques, S. L. Optical properties of biological tissues: a review. *Physics in Medicine and*
688 *Biology*. **58** (11), R37–R61 (2013).
689 40. Zhang, D., Slipchenko, M. N., Cheng, J.-X. Highly sensitive vibrational imaging by
690 Femtosecond Pulse Stimulated Raman Loss. *The Journal of Physical Chemistry Letters*. **2** (11),
691 1248–1253 (2011).
692 41. Hu, F., Shi, L., Min, W. Biological imaging of chemical bonds by stimulated Raman scattering
693 microscopy. *Nature Methods*. **16** (9), 830–842 (2019).
694 42. Ji, M. et al. Rapid, label-free detection of brain tumors with Stimulated Raman Scattering
695 Microscopy. *Science Translational Medicine*. **5** (201), 201ra119 (2013).
696 43. Freudiger, C. W. et al. Multicolored stain-free histopathology with coherent Raman imaging.
697 *Laboratory Investigation*. **92** (10), 1492–1502 (2012).
698 44. Lu, F.-K. et al. Label-free DNA imaging in vivo with stimulated Raman scattering microscopy.
699 *Proceedings of the National Academy of Sciences of the United States of America*. **112** (37),
700 11624–11629 (2015).
701 45. Yamakoshi, H. et al. Imaging of EdU, an Alkyne-tagged cell proliferation probe, by Raman
702 Microscopy. *Journal of the American Chemical Society*. **133** (16), 6102–6105 (2011).
703 46. van Manen, H.-J., Lenferink, A., Otto, C. Noninvasive imaging of protein metabolic labeling
704 in single human cells using stable isotopes and Raman Microscopy. *Analytical Chemistry*. **80**

(24), 9576–9582 (2008).
47. Zhang, L. et al. Spectral tracing of deuterium for imaging glucose metabolism. *Nature Biomedical Engineering*. **3** (5), 402–413 (2019).
48. Shi, L. et al. Optical imaging of metabolic dynamics in animals. *Nature Communications*. **9** (1), 2995 (2018).
49. Ahuja, C. S. et al. Traumatic spinal cord injury. *Nature Reviews Disease Primers*. **3** (1), 1–21 (2017).
50. Lassmann, H. Multiple sclerosis pathology. *Cold Spring Harbor Perspectives in Medicine*. **8** (3), a028936 (2018).

Figure1

Click here to access/download;Figure;Figure1.tif

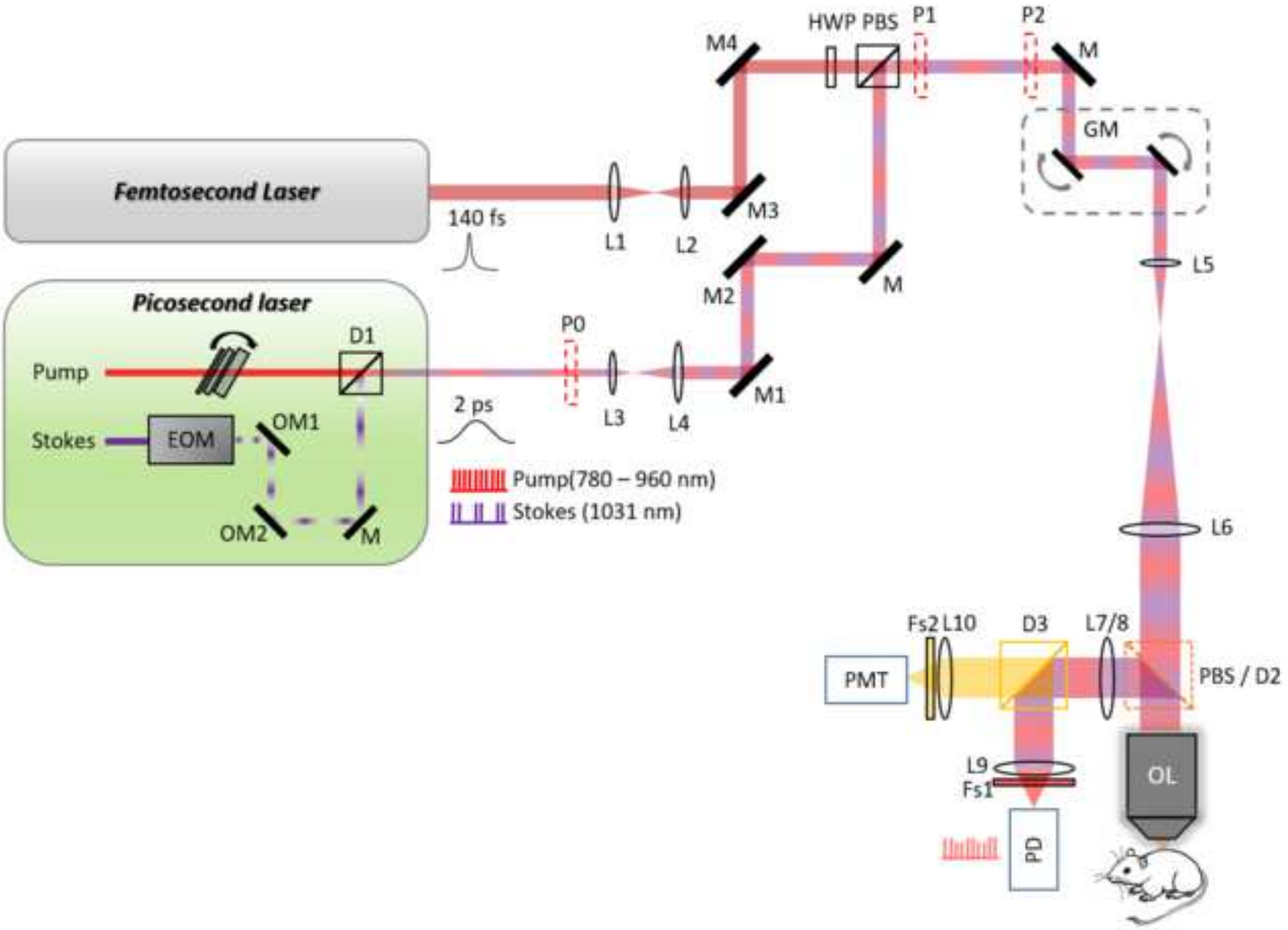

Figure2

Click here to access/download;Figure;Figure2.tif

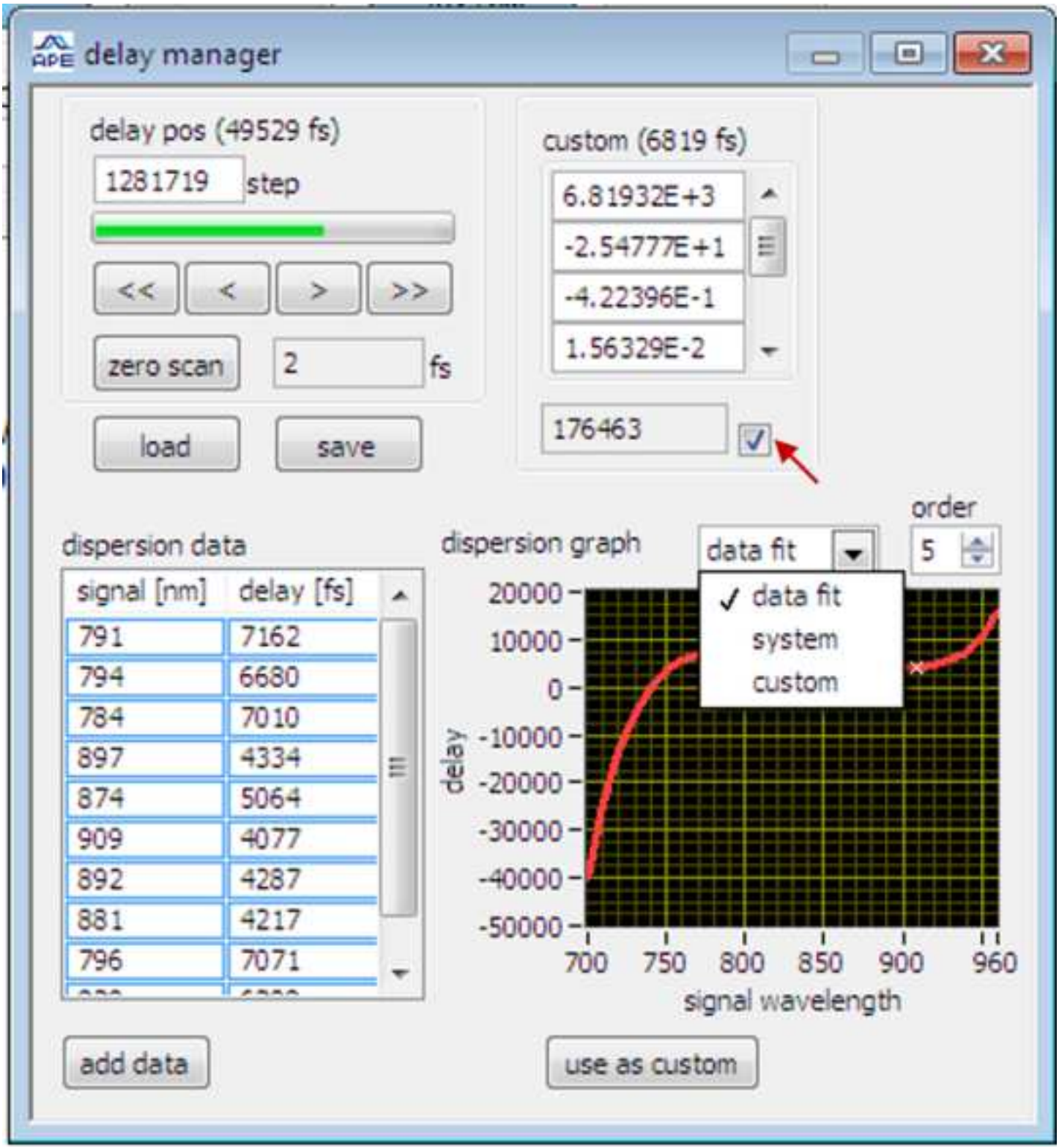

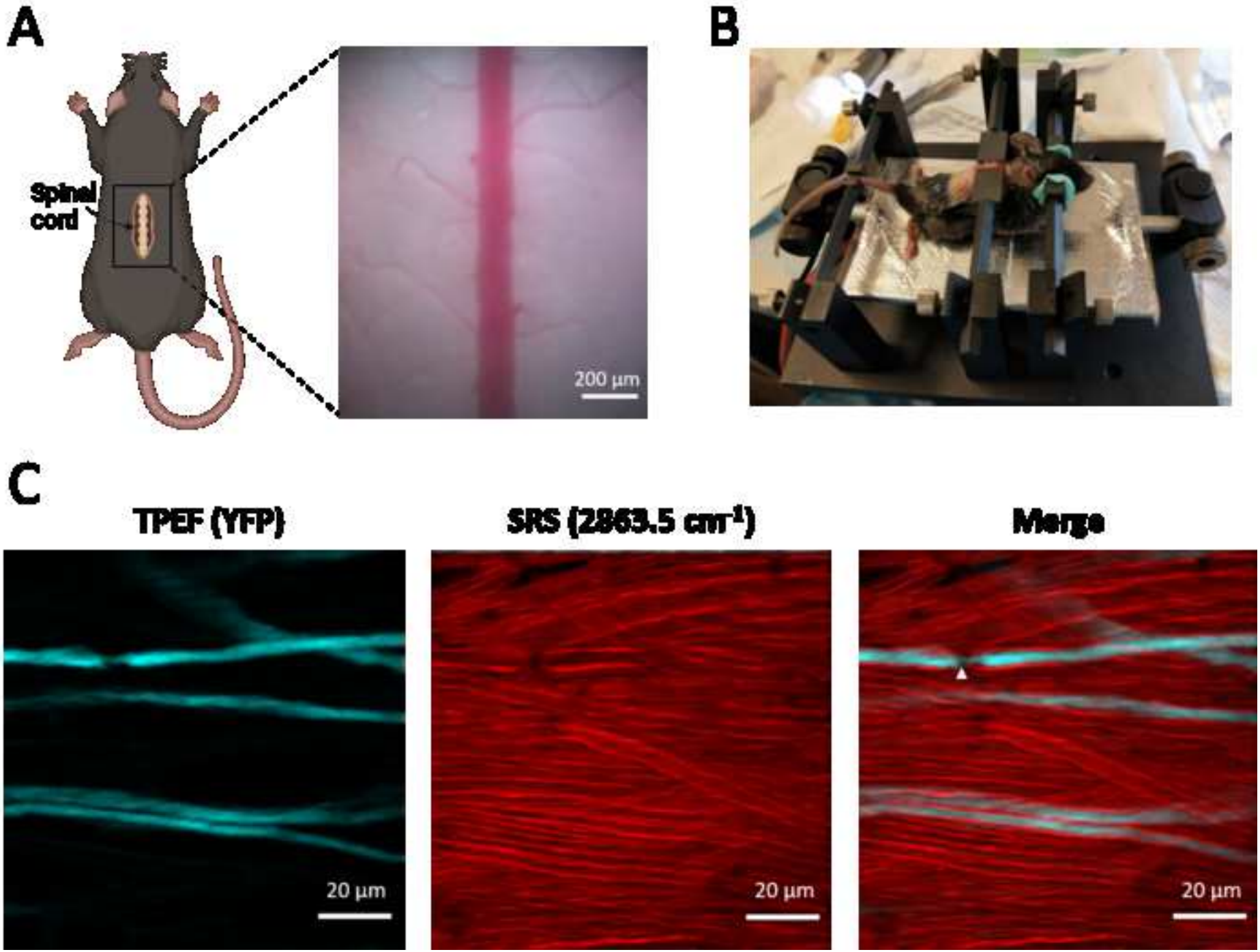

Table of material

Click here to access/download
Table of Materials
Material list_updated.xls

Title: ***In vivo* imaging of biological tissues with combined two-photon fluorescence and stimulated Raman scattering microscopy**

Author: Wanjie Wu, Xuesong Li, Jianan Y. Qu and Sicong He,

Dear Editor,

Thank you for considering our manuscript entitled "***In vivo* imaging of biological tissues with combined two-photon fluorescence and stimulated Raman scattering microscopy**" for publication in *Journal of Visualized Experiments*. We are most grateful to the reviewers for their time in reviewing our manuscript. We appreciate the reviewers' valuable and constructive comments to improve the quality of our manuscript.

We have revised the manuscript carefully and all the concerns from the reviewers have been addressed in the revised manuscript or in the responses to reviewers' comments. Enclosed please find the detailed responses (in black text) to the reviewer's comments (in blue text) and the indications of revisions in the manuscript (highlighted in grey). All the corresponding changes in the revised manuscript have been indicated as red text for your and the reviewer's convenience to locate the revisions.

Sincerely,

Sicong HE

Responses to Editorial comments

The authors agree with all the issues raised by the editor and all the concerns from the editor have been addressed in the revised manuscript or responses. We appreciate the editor's suggestions to improve the quality of our paper. The responses and revisions based on comments received are as follows:

Comment 1: *Please take this opportunity to thoroughly proofread the manuscript to ensure that there are no spelling or grammar issues.*

Response: Thanks for the suggestion. Spelling and grammar issues were checked and corrected throughout the manuscript.

Comment 2: *Please provide citations for the following lines: 85-91.*

Response: According to Reviewer #2 and Reviewer #3's suggestions that it is better to focus on one biological application, we removed the contents of adipose tissue imaging in the revised manuscript.

Comment 3: *Please define all abbreviations upon first use. For example: OPO, OM, etc.*

Response: Thanks for careful reading of our manuscript. We defined all abbreviations in the revised manuscript.

Revision: *Page 3, line 92-93:* "1.1. Use an integrated optical parametric oscillator (OPO) connected with a mode-locked Ytterbium fiber laser as the picosecond (ps) laser source for SRS imaging."

Page 3, line 96-98: "The Stokes beam is modulated at 20 MHz by a built-in electro-optical modulator (EOM) for SRS high-frequency (MHz) phase-sensitive detection."

Page 6, line 228-231: "2.2.2.2. Place an alignment plate P0 before L3 (Figure 1). Use an M2 hex key to adjust the optical mirror 1 (OM1) so that the Stokes beam center passes the through-hole of the alignment plate at the laser output port. Use the IR scope to confirm the position of the beam spot at P0 during adjustment."

Comment 4: *The Protocol should contain only action items that direct the reader to do something.*

Response: Thanks for the suggestion. We reorganized the protocol accordingly.

Comment 5: *JoVE cannot publish manuscripts containing commercial language. This includes trademark symbols (™), registered symbols (®), and company names before an instrument or reagent. Please remove all commercial language from your manuscript and use generic terms instead. All commercial products should be sufficiently referenced in the Table of Materials. For example: Kwik-Sil, etc.*

Response: We have removed all commercial language in the revised manuscript.

Comment 6: *Please revise the text to avoid the use of any personal pronouns (e.g., "we", "you", "our" etc.).*

Response: All personal pronouns were revised accordingly.

Comment 7: *Please add more details to your protocol steps. Please ensure you answer the "how" question, i.e., how is the step performed?*

Step 1.1.3: How was the output fed into the oscilloscope?

Step 1.2.1.1: How was the pump wavelength and power set? Please provide all associated steps.

Step 1.2.1.3: How was the positioning of I1 and I2 determined? How was the position of the laser beam checked?

Step 1.3.1.4: How were the imaging parameters set? What was the value used for the current experiment?

Step 1.3.1.5, 1.3.1.6: What are the various steps followed to tune the amplifier phase and to set the SRS signal to zero? Please mention all associated steps.

Line 284: Please shift the ethical statement to the beginning of the protocol.

Step 2.1.3, 2.2.1: How was proper anesthetization confirmed? Please specify the use of vet ointment on eyes to prevent dryness while under anesthesia.

Step 2.2.2: How was the mouse skin removed? Please mention all steps.

Step 3.1.19: Please mention the suture size.

Response: Thanks for the comments and suggestions. We added more details to the protocol steps in the revised manuscript.

Revision:

Page 4, line 158-160: "Connect the output port of the photodetector to the input port of an oscilloscope using a coaxial cable with Bayonet Neill-Concelman (BNC) connector to monitor the laser pulse."

Page 5, line 177-178: "Use OPO control software to set the wavelength of the pump beam to 796 nm, and set its power to the minimum (~20 mW) for optical alignment."

Page 5, line 186-187: "2.2.1.3 Place two alignment plates (P1 and P2 in Figure 1) on the optical path. Place P1 behind PBS at a distance of about 10 cm and place P2 behind P1 at a distance of about 30 cm."

Page 5, line 194-195: "2.2.1.5. Adjust mirror M1 to locate the ps laser beam center at the through-hole of P1. Use an IR scope to observe the position of the beam spot at P1 when adjusting the mirror M1.

Page 5, line 197-198: "2.2.1.6 Adjust mirror M2 to locate the ps laser beam center at the through-hole of P2. Use the IR scope to observe the position of the beam spot at P2 when adjusting the mirror M2."

Page 6, line 257-258: "2.3.1.2 Set the wavelength of the pump laser to 796 nm and the power of the pump and Stokes beam to be 15 mW and 25mW after the 25× objective lens, respectively.

Page 6-7, line 264-265: "2.3.1.3 Place the olive oil sample on the stage and adjust the focus of 25× objective into the sample."

Page 7, line 270-292: "2.3.1.4 Use the microscope control software to set the imaging parameters and use the lock-in amplifier control software to set a time constant value close to the pixel dwell time.

Note: the parameters for SRS imaging of olive oil are 512×512 pixels, 500 μm×500 μm field of view (FOV), 6.4 μs pixel dwell time, 10 μs time constant.

2.3.1.5 Scan the laser beam over the sample. Use the lock-in amplifier control software to tune the phase (0-180°) with a step size of 22.5° until the SRS signal intensity reaches the maximum.

Note: In this all-analog lock-in amplifier, the signal output is the In-Phase component which is dependent on the phase of the reference signal. The phase can be adjusted by the lock-in amplifier control software with 11-degree resolution, allowing to maximize the detected signal to within ~2%[12]. The lock-in amplifier gets out of phase once the sync signal is disrupted. The phase needs to be readjusted every time the sync signal is reestablished.

Step 2.3.1.6 Scan the sample with laser shutter closed. Use the lock-in amplifier control software to tune the offset value with a step size of 1mV until the average SRS signal is close to zero.

Note: the average SRS signal is estimated as the average intensity of all pixels in the SRS image, which is calculated automatically by the microscope control software. Offsets are useful for canceling unwanted phase-coherent signals."

Page 8, line 346-347: "Perform toe pinching to ensure deep anesthesia of the mouse. Supplement with half the original dose of the anesthetics as needed."

Page 8, line 352: "3.1.5 Apply ointment to the mouse eye to prevent corneal dryness."

Page 11, line 447: "4.19 Suture the skin with #6-0 surgical suture to close the wound."

Comment 8: *Please ensure that the highlighting is not more than 3 pages including headings and spacing*

Response: Thanks for the suggestion. We adjusted the highlighting contents to be less than 3 pages in the revised manuscript.

Comment 9: *Figures: Please mention all abbreviations used in the figure legends.*

Response: Abbreviations in the figure legend were revised accordingly.

Revision: *Figure 1 caption:* "**Figure 1. The schematic diagram of the TPEF-SRS microscope system.** Pump and Stokes beams are combined with a dichroic mirror (D1) in the picosecond (ps) laser. The ps beam and femtosecond (fs) beam are collimated and expanded/narrowed by a pair of lenses (L1, L2, and L3, L4 respectively) to match the 3 mm XY-scan galvo mirrors. The fs beam is rotated from horizontal to vertical polarization by a half-wave plate (HWP) and then combined with the ps beam by a polarizing beam splitter (PBS). The scanning mirrors and the rear pupil of the objective lens are conjugated by a telecentric scan lens L5 and an infinity-corrected tube lens L6. The laser beam is expanded by the scan and tube lens to fill the back aperture of the 25× objective. For stimulated Raman scattering (SRS) imaging, the backscattered pump beam collected by the objective is reflected by a PBS and directed to a large area (10mm×10mm) Silicone photodiode (PD). For two-photon imaging, the two-photon excited fluorescence (TPEF) signal is reflected by a dichroic beam splitter D2 to the photodetection unit. A current photomultiplier (PMT) module is used to detect the TPEF signal. L1-L10: lenses; OL: objective lens; D1-D3: dichroic mirrors; Fs1, Fs2: filter sets; M: mirrors; OM1, OM2: optical mirrors; P0-P2: alignment plates."

Comment 10: *Figure 3: Please provide scale bar for all microscope images.*

Response: Scale bars were added to all microscope images in the revised manuscript.

Comment 11: *Please also include in the Discussion the following in detail along with citations:*

a) Critical steps within the protocol

b) Any limitations of the technique

Response: Thanks for the suggestions. We added discussions along with citations on the critical steps within the protocol and limitations of this technique in the revised manuscript.

Revision: *Page 12, line 512-526:* "For SRS imaging, though pump and Stokes beams are temporally and spatially overlapped inside the OPO, this overlapping can be disrupted after passing through the microscope system. Therefore, both spatial and temporal optimization of the colocalization of the pump and Stokes beams is necessary and critical to achieve optimal SRS imaging. Phase and offset adjustment are also important to get the maximal SRS signal output with the all-analog lock-in amplifier setup[12]. In addition, initial calibration of the temporal delay between the Stokes and pump beams at different wavelengths would be helpful for fast SRS spectra sweeping and imaging at various Raman shifts. For TPEF-SRS imaging, strict spatial overlapping of the ps and fs beams after the combination is important to avoid any FOV shift when switching the two imaging modes. Therefore, in this TPEF-SRS microscope, totally three beams are involved in the spatial colocalization. Firstly, the ps pump beam and fs beam are aligned, to make sure they both pass the center of the microscope cage system. Then using the pump beam as a reference, the Stokes beam position is adjusted accordingly to achieve strict spatial colocalization. Each alignment procedure requires several trials to reach the optimum."

Page 12-13, line 530-541 "In this protocol, TPEF and SRS imaging at the same location are performed sequentially with 1 s interval. Motion artifacts during spinal cord imaging may cause an imperfect merge of the TPEF and SRS images, which limits the capability of this method for imaging highly dynamic processes or tissues largely affected by the breath and heartbeat of animals. One possible solution is to collect the ps laser excited two-photon fluorescence during SRS imaging[9]. However, this method is only applicable to the biological structures with strong fluorescence signals since the ps pulse has a much lower excitation efficiency compared to the fs pulse[20]. Alternatively, the motion problem can be solved by using a fs-SRS system[21, 22], where the fs laser source allows exciting the

SRS and TPEF signals simultaneously in an efficient way, at the expense of low spectral resolution of SRS imaging. As shown in Figure 3, this registration strategy works well when no significant motion occurs during the SRS and fluorescence imaging."

Responses to reviewers' comments

The authors agree with most of the issues raised by the reviewers and all the concerns from the reviewers have been addressed in the revised manuscript or responses. We appreciate the reviewers' suggestions to improve the quality of our paper. The responses and revisions based on comments received are as follows:

RESPONSES TO THE COMMENTS FROM REVIEWER #1:

General: *A number of papers concerning SRS and TPE implementations have already reported in JOVE and the combination of these two techniques, using two different laser system, is not challenging and above all no significant news are proposed. Therefore, in my opinion, this paper doesn't deserve to be published in a journal whose aim is to bring to life details of cutting edge technologies. Concerning TPE implementation no new details in its implementation with respect to other ones are pointed out. For SRS, being the two difficult conditions to get in SRS implementation, i.e. spatial and temporal alignment, essentially provided by the laser system, the implementation presented is a simplified one. Details about the implementation of high-frequency modulation transfer method are missing. SRS is a shot noise limited technique, but this crucial point is not discussed into the paper and no evidence are reported that this condition is achieved. In addition the synchronization of the signal acquired by the phase-sensitive detection scheme, with the beam positioned onto the sample monitored by the scan head of the microscope is completely missing. This is a typical obstacle for SRS implementation. Again, no details about microscope are provided, if it is a home built or a commercial system. Of course this difference is important. If the used microscope is a commercial one, the only key experimental point would be colocalization of the ps and fs beams, but this is not enough for publication. Details about images time acquisition pixel dwell time and integration time should be reported to demonstrate that the techiniques are fast enough to allow in vivo imaging.*

Response: We appreciate the reviewer's thorough assessment of our manuscript. We have followed the reviewer's comments to revise our manuscript accordingly.

Comment 1: *In section 1.2.3 Setup of the detection optical path and electronics. The Filter should be linked to the list of material*

Response: Thanks for the suggestion. All the filters have been listed in the Table of Materials with the same name as in the protocol and figure for cross reference.

Comment 2: *In section 1.3.1 Phase adjustment of the lock-in amplifier. The results obtained by lock in should not depend on phase. Why is this optimisation process necessary?*

Response: Good question. The lock-in amplifier (LIA) used in our microscope system is an all-analog device designed based on the Ref below. This LIA is designed for high-speed SRS imaging and thus has no digital signal processing module to directly calculate the signal amplitude as other LIA device (e.g. SR844, Stanford Research Systems) does. Therefore, the output signal is the In-Phase component, which is dependent on the phase difference between the signal and reference. In our case, the phase of the reference is adjusted using the LIA control software so that the maximal SRS signal can be obtained.

Ref:

Saar, B.G., Freudiger, C.W., Reichman, J., Stanley, C.M., Holtom, G.R., Xie, X.S. Video-Rate Molecular Imaging in Vivo with Stimulated Raman Scattering. Science. 330 (6009), 1368–1370, doi: 10.1126/science.1197236 (2010).

Revision: *Page 7, line 280-284:* "In this all-analog lock-in amplifier, the signal output is the In-Phase component which is dependent on the phase of the reference signal. The phase can be adjusted by the lock-in amplifier control software with 11-degree resolution, allowing to maximize the detected signal to within ~2%[12]. The lock-in amplifier gets out of phase once the sync signal is disrupted. The phase needs to be readjusted every time the sync signal is reestablished."

Comment 3: *In section 1.3.1.6 Scan the sample with laser shutter closed. Tune the offset value until the average SRS signal is close to zero. How this average SRS signal is estimated? Do you measure Noise with LIA or calculate noise from images?*

Response: The average SRS signal was estimated as the average intensity of all pixels in the SRS image, which was calculated automatically by the control software when the SRS image was captured. We didn't measure noise with LIA or from images.

Revision: *Page 7, line 286-292:* "Scan the sample with laser shutter closed. Use the lock-in amplifier control software to tune the offset value with a step size of 1mV until the average SRS signal is close to zero.

Note: the average SRS signal is estimated as the average intensity of all pixels in the SRS image, which is calculated automatically by the microscope control software. Offsets are useful for canceling unwanted phase-coherent signals."

Comment 4: *The delay between pump and probe should not depend on wavelength. If not, explain why?*

Response: Thanks for pointing out the issue. The delay between pump and probe laser depends on the optical path difference (OPD):

$$\mathrm{OPD} = (n_{probe} - n_{pump}) \times \mathrm{L}$$

where n_{probe} and n_{pump} are the refractive index of optical components at the wavelengths of probe and pump lasers, respectively, while L represents the length of optical path or thickness of optical components in the microscope system. As the refractive index of glass changes with the light wavelength [Ref below], the OPD varies when we adjust the probe wavelength while maintaining the pump wavelength (1031nm). Therefore, the delay between the two beams depends on wavelength and needs to be calibrated prior to SRS imaging.

Ref:

1. Chartier, Germain. *Introduction to optics*. Springer Science & Business Media, 2005. (Chapter3.3, page 63-64)

Revision: *Page 7, line 296-297*: "Note: The delay between the pump and Stokes beam is related to the optical path difference, which is determined by the dispersion of optical components in the microscope system."

Comment 5: *In discussion, you claim: As a result, though the backscattered signal collection by objective is less efficient than that by directly objective placing an annular photodetector in front of the SRS images (512 X 512 pixels) of the spinal cord and adipose tissue with a high signal-to-noise ratio can 529 be acquired with 1~2 s integration time. The point is that if you use a PBS, you detect a scattered beam with a different polarization with respect to the incident beam. Please explain how this different polarization can influence the efficiency of SRS detected signal.*

Response: Good question. Since the backscattered SRS signal has various polarizations, we used a PBS to distinguish the incident light and backscattered light. The polarization axis of PBS is parallel to the incident lasers to maximize the transmittance of excitation light. The SRS signal, backscattered from the tissue, has shifted polarization, and can thus be partially reflected by the PBS and

collected by the photodiode. In contrast, the annular photodetector can collect most of backscattered SRS signals regardless of polarization, thus allowing higher collection efficiency.

Revision: *Page 3, line 121-122:* "Part of the back-scattered SRS signal is lost when passing through the PBS as a result of its randomly shifted polarization."

Comment 6: *The aim of your work is to perform in vivo experiment, but your experimental set up imposes that TPEF and SRS imaging were performed sequentially at the same location. This a fundamental limitation for in vivo measurements and I think that you porposed solution is not a suitable relief.*

Response: Good question. We used a motorized flipper and custom software to switch the imaging models. The total time for sequential TPEF imaging, model switching, and SRS imaging are about 3s. For *in vivo* imaging in brain or other tissues which are less affected by the breath and heartbeat of the mouse, this sequential imaging approach should not be a problem since the 1-s switch time is short enough to avoid inter-frame motion artifacts. In contrast, spinal cord imaging is largely affected by the breath and heartbeat motion, and we indeed observe imperfect merge between SRS and fluorescence images, especially when the mice were not well anesthetized. One possible solution is to collect the ps laser excited two-photon fluorescence during SRS imaging simultaneously. However, because ps pulse has much lower excitation efficiency compared to the fs pulse, this solution is only applicable to the biological structures with strong fluorescence signal like the YFP-labeled axons in our case. Alternatively, if spectral resolution of SRS imaging is not highly demanded, a fs-SRS-TPEF system can be used to capture the SRS and fluorescence images simultaneously. Another solution is to use the ps laser excited fluorescence obtained during SRS imaging as a reference to register the fs fluorescence images. As shown in Figure 3, this registration strategy works well if no significant motion occurs during the SRS and fluorescence imaging. We have added the discussion in the revised manuscript.

Revision: *Page 13, line 530-541:* "In this protocol, TPEF and SRS imaging at the same location are performed sequentially with 1 s interval. Motion artifacts during spinal cord imaging may cause an imperfect merge of the TPEF and SRS images, which limits the capability of this method for imaging highly dynamic processes or tissues largely affected by the breath and heartbeat of animals. One possible solution is to collect the ps laser excited two-photon fluorescence during SRS imaging[9]. However, this method is only applicable to the biological structures with strong fluorescence signals since the ps pulse has a much lower excitation efficiency compared to the fs pulse[20]. Alternatively, the motion problem can be

solved by using a fs-SRS system[21, 22], where the fs laser source allows exciting the SRS and TPEF signals simultaneously in an efficient way, at the expense of low spectral resolution of SRS imaging. As shown in Figure 3, this registration strategy works well when no significant motion occurs during the SRS and fluorescence imaging."

Comment 7: *In introduction, the first paragraph concerning comparison of SRS with CARS and Raman spectroscopy should be removed. This comparison has been reported too many times in literature (see for example several SRS review papers). A preliminary description of step by step implementation should be added, in which missing crucial points are pointed out and above all what are the novelty of this combination of techniques should be pointed out.*

Response: Agree. We removed the contents on the comparison of SRS with CARS and Raman spectroscopy. More details on the implementation of the home-built microscope system were added in the revised manuscript.

Revision: *Page 2-4, line 81-146:* "

Note: All animal procedures performed in this work are conducted according to the guidelines of the Laboratory Animal Facility of the Hong Kong University of Science and Technology (HKUST) and have been approved by the Animal Ethics Committee of HKUST. Safety training for laser handling is required to set up and operate the TPEF-SRS microscope. Always wear laser safety goggles with appropriate wavelength range when dealing with laser.

1. Instrumental setup of the TPEF-SRS microscope.

Note: The setup schematic of the home-built TPEF-SRS microscope system is shown in Figure 1. This part introduces major procedures for the setup of the TPEF-SRS microscope system

1.1. Use an integrated optical parametric oscillator (OPO) connected with a mode-locked Ytterbium fiber laser as the picosecond (ps) laser source for SRS imaging.

Notes: OPO outputs a Stokes beam (1031nm) and a pump beam (tunable from 780nm to 960nm) with 2-ps pulse duration and 80 MHz repetition rate. The Stokes beam is modulated at 20 MHz by a built-in electro-optical modulator (EOM) for SRS high-frequency (MHz) phase-sensitive detection.

1.2. Use a femtosecond (fs) Ti: sapphire laser as the laser source for TPEF imaging.

1.3. Use a pair of lenses (L1 and L2) to collimate and adjust the size of fs beam to be 3 mm.

1.4. Use a pair of achromatic doublets (L3 and L4) to collimate the ps laser beam and expand its diameter to be 3 mm.

1.5. the polarization of fs laser beam from p polarization to s polarization using a half-wave plate.

1.6. Combine the two laser beams with a polarizing beam splitter (PBS).

1.7. Add a pair of 3 mm XY-scan galvo mirrors behind the PBS for beam scanning.

1.8. Use a telecentric scan lens L5 and an infinity-corrected tube lens L6 to conjugate the scanning mirror and the rear pupil of the 25× objective lens. The laser beam is also expanded by the scan lens and tube lens to fill the back aperture of the objective.

1.9. Place a PBS or dichroic mirror (D2) between the tube lens and objective lens for SRS or fluorescence signal collection. PBS and D2 are switchable by using a motorized flipper.

Note: part of the back-scattered SRS signal is lost when passing through the PBS as a result of its randomly shifted polarization.

1.10. Use a pair of lenses (L7 and L9) to narrow the detection beam and conjugate the rear pupil of 25× objective lens with a photodiode sensor.

1.11. Use a pair of lenses (L8 and L10) to narrow the detection beam and conjugate the rear pupil of 25 × objective with the detection surface of the photomultiplier (PMT).

1.12. Use a dichroic mirror (D3) to separate the detection path of fluorescence and SRS signals.

1.13. Place a filter set (Fs1) in front of the photodiode detector to block the Stokes laser and pass the pump beam only.

1.14. Place a filter set (Fs2) in front of the PMT detector to pass the target fluorescence signal only.

1.15. Connect the PMT to a current amplifier for signal amplification.

1.16. Connect the photodiode to a lock-in amplifier.

1.17. Connect the sync signal from the built-in EOM output to the reference input of the lock-in frequency for SRS signal demodulation.

1.18. Connect the PMT amplifier and lock-in amplifier outputs to the data acquisition module.”

RESPONSES TO THE COMMENTS FROM REVIEWER #2:

General: *In this manuscript, Wu and colleagues aim to illustrate two methods (1) how to setup a homemade system combining 2P fluorescence and SRS techniques and, (2) how to record images of biological tissues in living animals. Overall, these methods are of general interest for the engineers developing noncommercial systems and biologists, respectively.*

My main concern comes from this dual goal in a limited space (the article by itself) and time (the expected video), mainly because important information, explanations and experimental details are lacking for setting up the microscope and recording the data. One option would have been to choose either method, but not both at the same time.

Response: We appreciate the reviewer's thorough assessment of our manuscript and positive opinion about our work. We have followed the reviewer's comments to revise our manuscript accordingly.

Comment 1: *The described procedure is highly dependent on the design homemade installation. Consequently, the authors have to provide a detailed protocol for building this microscope, but the current version is not explicit enough. At a first step, one should expect a thorough explanation of the function of the different constituents and a description of the procedure to assemble them. This part should not necessarily be illustrated in the video, but only detailed in the text.*

Response: Thanks for the reviewer's suggestions. We added more detailed descriptions on the implementation of our home-built microscope system in the revised manuscript.

Revision: *Page 2-4, line 81-146:* "

Note: All animal procedures performed in this work are conducted according to the guidelines of the Laboratory Animal Facility of the Hong Kong University of Science and Technology (HKUST) and have been approved by the Animal Ethics Committee of HKUST. Safety training for laser handling is required to set up and operate the TPEF-SRS microscope. Always wear laser safety goggles with appropriate wavelength range when dealing with laser.

1. Instrumental setup of the TPEF-SRS microscope.

Note: The setup schematic of the home-built TPEF-SRS microscope system is shown in Figure 1. This part introduces major procedures for the setup of the TPEF-SRS microscope system

1.1. Use an integrated optical parametric oscillator (OPO) connected with a mode-locked Ytterbium fiber laser as the picosecond (ps) laser source for SRS imaging.

Notes: OPO outputs a Stokes beam (1031nm) and a pump beam (tunable from 780nm to 960nm) with 2-ps pulse duration and 80 MHz repetition rate. The Stokes beam is modulated at 20 MHz by a built-in electro-optical modulator (EOM) for SRS high-frequency (MHz) phase-sensitive detection.

1.2. Use a femtosecond (fs) Ti: sapphire laser as the laser source for TPEF imaging.

1.3. Use a pair of lenses (L1 and L2) to collimate and adjust the size of fs beam to be 3 mm.

1.4. Use a pair of achromatic doublets (L3 and L4) to collimate the ps laser beam and expand its diameter to be 3 mm.

1.5. the polarization of fs laser beam from p polarization to s polarization using a half-wave plate.

1.6. Combine the two laser beams with a polarizing beam splitter (PBS).

1.7. Add a pair of 3 mm XY-scan galvo mirrors behind the PBS for beam scanning.

1.8. Use a telecentric scan lens L5 and an infinity-corrected tube lens L6 to conjugate the scanning mirror and the rear pupil of the 25× objective lens. The laser beam is also expanded by the scan lens and tube lens to fill the back aperture of the objective.

1.9. Place a PBS or dichroic mirror (D2) between the tube lens and objective lens for SRS or fluorescence signal collection. PBS and D2 are switchable by using a motorized flipper.

Note: part of the back-scattered SRS signal is lost when passing through the PBS as a result of its randomly shifted polarization.

1.10. Use a pair of lenses (L7 and L9) to narrow the detection beam and conjugate the rear pupil of 25× objective lens with a photodiode sensor.

1.11. Use a pair of lenses (L8 and L10) to narrow the detection beam and conjugate the rear pupil of 25 × objective with the detection surface of the photomultiplier (PMT).

1.12. Use a dichroic mirror (D3) to separate the detection path of fluorescence and SRS signals.

1.13. Place a filter set (Fs1) in front of the photodiode detector to block the Stokes laser and pass the pump beam only.

1.14. Place a filter set (Fs2) in front of the PMT detector to pass the target fluorescence signal only.

1.15. Connect the PMT to a current amplifier for signal amplification.

1.16. Connect the photodiode to a lock-in amplifier.

1.17. Connect the sync signal from the built-in EOM output to the reference input of the lock-in frequency for SRS signal demodulation.

1.18. Connect the PMT amplifier and lock-in amplifier outputs to the data acquisition module."

Comment 2: *Actually, the procedure to align and optimize the setup is unclear. For instance, line 136: "start the microscope control software": is it a homemade interface or a commercial one? Line 180: where are OM1 and OM2 in figure 1; Line 184, "remove the iris": Which one? Line 204: this note comes too late; Line 220-221: for what objective lens, 10X, 25X? Etc…*

Response: Thanks for pointing out the issues. The microscope control software is a homemade interface developed using C# language.

OM1 and OM2 are two optical mirrors inside the optical parametric oscillator (OPO), which have been added in the revised Figure 1.

The iris mentioned in Line 184 was placed close to the OPO output. We described the iris as alignment plate which should be more appropriate and mark it as P0 in the revised Figure 1.

The content in Line 204 has been moved to the part 1 of the protocol.

The objective mentioned in Line 220-221 is 25×.

We revised the manuscript according to the reviewer's comments and added detailed descriptions on the procedures of system alignment and optimization.

Revision: *Page 5, line 184:* "Note: the microscope control software is a homemade interface."

Figure 1: OM1 and OM2 were added in the figure.

Page 6, Line 236-238: "2.2.2.3 Remove the alignment plate P0 and use the M2 hex key to adjust the OM2 so that the center of the Stokes beam colocalizes with the reference mark."

Page 4, Line 139: "1.15. Connect the PMT to a current amplifier for signal amplification."

Page 4, Line 141-146: "1.16. Connect the photodiode to a lock-in amplifier.

1.17. Connect the sync signal from the built-in EOM output to the reference input of the lock-in amplifier for SRS signal demodulation.

1.18. Connect the PMT amplifier and lock-in amplifier outputs to the data acquisition module."

Page 6, Line 257-258: "Set the wavelength of the pump laser to 796 nm and the power of the pump and Stokes beam to be 15 mW and 25 mW after the 25× objective lens, respectively."

Comment 3: *The procedure to analyze the date is really incomprehensible (Lines 273-275)*

Response: Thanks for pointing out the issue. The data analysis procedures in Lines 273-275 are performed by clicking buttons on the OPO control software. To make it more comprehensible, we added a figure (Figure 2) to show the interface of the delay manager control. These procedures will also be recorded by video afterwards.

Revision: Figure 2 was added

Figure 2 caption: "**Figure 2. Interface of the delay manager on the OPO control software.** The red arrow indicates the checking box for applying the calibrated delay data."

Page 7, Line 306: "2.3.2.1. Open the delay manager dialog (Figure 2) in the OPO control software."

Comment 4: *Moreover, laser safety procedures are lacking, especially when a femtosecond Ti:sapphire laser is used at not visible wavelengths.*

Response: Thanks for pointing out this important safety issue. We wear laser goggles for eye protection when handling the laser. This important issue has been added in our revised manuscript.

Revision: *Page 2, line 83-85:* "Safety training for laser handling is required to set up and operate the TPEF-SRS microscope. Always wear laser safety goggles with appropriate wavelength range when dealing with laser."

Comment 5: *If the main objective is to promote the use of this imaging system, more space can be obtained to detail the setup by choosing only one of the two biological models to illustrate and validate the interest of this method.*

Response: Agree. We removed the second biological model of adipose tissue imaging, and focused on the use of microscope system in the revised manuscript.

Comment 6: *I assume that all surgical preparation is performed under anesthesia conditions that are not mentioned here.*

Response: Thanks for the comment. Actually we mentioned the anesthesia procedures in Line 335-336. We added description on how to confirm proper anesthetization in the revised manuscript.

Revision: *Page 8, line 346-347:* "Perform toe pinching to ensure deep anesthesia of the mouse. Supplement with half the original dose of the anesthetics as needed."

Comment 7: *Again, laser safety procedures are lacking, especially when a femtosecond Ti:sapphire laser is used at not visible wavelengths.*

Response: Thanks again for pointing out this issue. We have added laser safety procedures in the revised protocol.

Revision: *Page 2, line 83-85:* "Safety training for laser handling is required to set up and operate the TPEF-SRS microscope. Always wear laser safety goggles with appropriate wavelength range when dealing with laser."

RESPONSES TO THE COMMENTS FROM REVIEWER #3:

General: *This review introduces the detailed procedures of in vivo imaging of biological tissues with combined two-photon fluorescence and stimulated Raman scattering microscopy.*

Response: We appreciate the reviewer's positive opinion about our work. We have followed the reviewer's comments to revise our manuscript accordingly.

Comment 1: *This paper covers both spinal cord imaging and white fat tissue imaging, which belong to very different areas. In my opinion, I suggest the paper focuses on one application.*

Response: Thanks for the suggestion. We removed the second application of adipose tissue imaging in the revised manuscript.

Comment 2: *We usually use 2850cm-1 to image CH vibration in lipids instead of 2863.5cm-1.*

Response: Thanks for the comment. We used 2863.5 cm^{-1} to image the myelin based on its SRS spectrum in the C-H region of which the SRS peak is observed at 2863.5 cm^{-1}. The difference between the 2850 cm^{-1} and 2863.5 cm^{-1} in the spectral domain is <1 nm, which is very close. For C-H vibration in lipids, the corresponding Raman peak varies among different lipid samples, determined by their specific molecular structures, as shown in the Ref below. Therefore, this difference in wavenumber may result from the different sample used. We added an explanation on the wavenumber to avoid any confusion in the revised manuscript.

Ref:

Czamara, K., Majzner, K., Pacia, M.Z., Kochan, K., Kaczor, A., Baranska, M. Raman spectroscopy of lipids: a review: Raman spectroscopy of lipids. Journal of Raman Spectroscopy. 46 (1), 4–20, doi: 10.1002/jrs.4607 (2015).

Revision: *Page 10, line 400-402:* "Note: Spinal cord SRS imaging is performed at the wavenumber of 2863.5 cm^{-1}, which corresponds to the Raman peak of myelin sheaths at the carbon-hydrogen region based on the measured SRS spectra."

Comment 3: *The work used a series of different laser power for different imaging experiments. Please explain how to decide the laser power in more details.*

Response: Thanks for pointing out this power issue. There is a tradeoff between the signal intensity and tissue damage when we determine the laser power for optical

imaging. For two-photon fluorescence imaging, strong fluorescence signal can be acquired with low laser power (10mW) due to the bright fluorescence labelling. However, it is not the case for label-free SRS imaging, which usually requires higher laser power to acquire good image contrast, especially for this epi detection mode used in this protocol. After test, we found that the current power condition (60mW Pump beam, 75mW Stokes beam) allows high imaging contrast with myelin sheaths clearly visualized and at the same time, tissue damage was not observed. In fact, the laser power we used is comparable to the previous studies on in vivo SRS imaging of myelin (Ref below). We added discussion on the laser power in the revised manuscript.

Ref:

Hu, C.-R., Zhang, D., Slipchenko, M.N., Cheng, J.-X., Hu, B. Label-free real-time imaging of myelination in the Xenopus laevis tadpole by in vivo stimulated Raman scattering microscopy. Journal of Biomedical Optics. 19 (8), 086005, doi: 10.1117/1.JBO.19.8.086005 (2014).

Revision: *Page 10, line 402-404:* "The laser power is determined to ensure high-resolution and high-contrast spinal cord images in both fluorescence and SRS imaging modalities. Tissue damage is not observed under the current imaging conditions."